THE JOURNAL OF PHYSICAL CHEMISTRY B

Article

pubs.acs.org/JPCB

Rheology of Disentangled Multiwalled Carbon Nanotubes Dispersed in Uncured Epoxy Fluid

Kevin L. White,[†,§] Peng Li,[†,§] Yasuhiro Sumi,[‡] and Hung-Jue Sue*[,†]

[†]Polymer Technology Center, Department of Mechanical Engineering, Texas A&M University, College Station, Texas 77843, United States

[‡]Process Research Laboratory, Corporate R&D Division, Kaneka Corporation, Takasago-cho, Takasago-shi, Hyogo 676-8688, Japan

Supporting Information

ABSTRACT: The rheological behaviors of clustered and disentangled multiwalled carbon nanotubes (MWCNTs) dispersed in a stable, non-reactive Newtonian epoxy fluid have been investigated. Suspensions of untreated and chemically oxidized MWCNTs in epoxy show strong rate-dependent behavior and long-time elastic response that is characteristic of a flocculated microstructure. Suspensions of disentangled MWCNTs in epoxy were prepared by a functionalization reaction with nitrobenzene, and show distinct rheological behavior that is attributed to the motion and rotation of the individual nanoparticles. Characteristic features of the disentangled MWCNTs in epoxy are a lack of low-frequency plateau in storage modulus and shear thickening behavior at high shear rate. The rheological behavior is discussed on the basis of continuum-level predictions for the motion of individual, semiflexible fibers under shearing flows. Implications of MWCNT disentanglement on fundamental study and applications of MWCNT-filled systems are discussed.

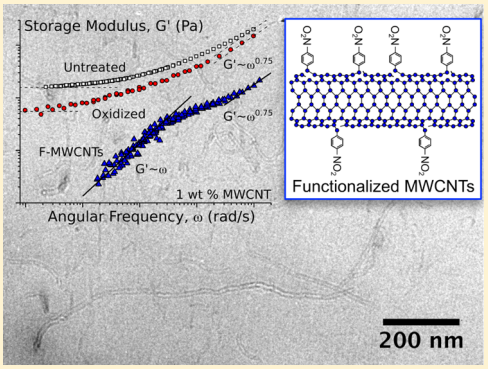

INTRODUCTION

Multiwalled carbon nanotubes (MWCNTs) are high aspect ratio, fiber-like nanoparticles that show an exceptional combination of mechanical, electrical, and thermal properties.[1−3] Individual MWCNTs tend to aggregate into mechanically cohesive flocs that are challenging to disperse without damaging the nanoparticle structure or modifying the nature of interaction with the suspending medium. As a result, it is challenging to clearly relate macroscale properties of polymer−MWCNT nanocomposites to particle-level attributes. Bauhofer et al.[4] recently showed that, even if MWCNT clusters are adequately dispersed in the polymer matrix through mechanical processing, the rheology of the nanocomposite tends to recover with time and approaches a limiting value independent of the initial dispersion state. This finding, and others that reported a similar convergence of properties with time after mechanical treatment,[5−7] suggests that most approaches to integrate MWCNTs in polymeric or fluid media result in a thermodynamically unstable dispersion state.

One major consequence of the lack of processing methods suitable to achieve a stable dispersion is that the majority of experimental results reflect properties dominated by the clusters rather than individual MWCNTs. It is unclear whether individual dispersion is needed for most applications, and in some situations, a controlled degree of aggregation has been reported to provide a desirable combination of properties.[8−12] If the aggregate structure is relatively well-defined and reproducible, this type of self-assembling system may provide a useful route to tailor properties across length scales.[13] However, unambiguous relationships between particle-level properties and desired macroscale response cannot be reasonably developed in these cases. Fundamental structure−property relationships are needed to identify mechanisms responsible for changes in bulk response, and to guide approaches to most effectively utilize this unique class of nanoparticles.

In this work, as-received MWCNT clusters are disentangled to the individual particle level following reaction with 4-nitroaniline in acetonitrile solution. The functionalized MWCNTs (F-MWCNTs) are shown to uniformly disperse in organic solvent as individual nanoparticles. The F-MWCNTs remain disentangled and well dispersed after redispersion in epoxy at 1 wt % concentration. The rheological behavior is compared with the response of suspensions containing clustered MWCNTs to show the role of disentanglement in the fluid response. Ongoing work is focused on relating these properties to processing conditions and behavior in solid-state nanocomposites. An epoxy fluid was used because of its good stability and limited reactivity with the MWCNTs at elevated temperature, which enables the use of time−temperature superposition (TTS) to identify changes in relaxation behavior. The epoxy has sufficient viscosity to introduce significant

Received: November 9, 2013
Revised: December 8, 2013
Published: December 16, 2013

hydrodynamic stresses during shearing. Any change in dynamics or organization of the suspending fluid at the nanoparticle interface should be negligible at the concentrations investigated in this work, and the size difference between the MWCNTs and the epoxy molecules should be sufficient to neglect any finite size effects. The flow properties of nanoparticle-filled epoxies are of practical importance because of their widespread use in resin transfer molding (RTM) and coating applications.[9,14−16]

EXPERIMENTAL SECTION

Materials. MWCNTs (Sigma-Aldrich) with 5−15 graphene wall average, >90% carbon basis, 2−6 nm inner diameter, 10−15 nm outer diameter, and length 0.1−10 μm were suspended inside of a diglycidyl ether of bisphenol F (DGEBF) epoxy fluid, EPIKOTE 862 (Hexion Specialty Chemicals, Inc.). Sigma-Aldrich reported the MWCNT density to be 2.1 g/cm^3. The density of the epoxy fluid was reported to be 1.16 g/cm^3.

Treatment and Dispersion of Clustered MWCNTs. Suspensions of clustered MWCNTs were prepared following the procedure described in our previous work.[8] The as-received MWCNTs were dispersed in acetone by ultrasonication for 1 h. The epoxy was added to the mixture and dissolved at room temperature. The mixture was sonicated for 15 min and dried by rotary evaporation at 80 °C. Samples were collected and dried in a vacuum oven overnight to remove any remaining solvent.

Functionalization and Dispersion of Disentangled MWCNTs. As-received MWCNTs were pretreated in a mixture of concentrated sulfuric and nitric acids (3:1 ratio by volume) in a sonication bath (Branson 2510) for 1.5 h at room temperature. DI water was added to dilute the acid solution, and the mixture was sonicated for an additional 2 h. Oxidized MWCNTs (O-MWCNTs) were isolated using a polyvinylidene difluoride filter membrane (Millipore, 0.45 μm pore size) under a vacuum, and were washed several times with DI water until the pH was nearly neutral. A 70 mg portion of O-MWCNT was mixed in 140 mL of SDBS aqueous solution (1 wt %) and sonicated for 4 h at room temperature. After sonication, the SDBS/O-MWCNT solution was added to a homogeneous solution of 140 mL of acetonitrile containing 3 g of nitroaniline. Under a nitrogen atmosphere, 3 mL of isoamyl nitrite was slowly added dropwise to the solution. The mixture was heated to 70 °C and mechanically stirred for 12 h. The mixture was filtered and washed with DI water and acetone several times. The recovered nanotubes, referred to here as F-MWCNTs, were redispersed in acetone at a concentration of 0.5 mg/mL. The epoxy fluid was added to the acetone/F-MWCNT solution at room temperature to achieve the desired concentration. The mixture was sonicated for 15 min and dried by rotary evaporation at 80 °C. Samples were collected and dried in a vacuum oven overnight to remove any remaining solvent.

Characterization. Thermogravimetric analysis (TGA) of samples was carried out in a nitrogen atmosphere using a Q500-TGA instrument (TA Instruments). The ramp rate was 10 °C/min. Fourier transform infrared spectroscopy in attenuated total reflectance mode (FTIR-ATR) was performed using a Nicolet Avatar 360 instrument. Absorbance was measured between 400 and 4000 cm^{-1}, with a resolution of 4 cm^{-1}.

The morphology of the modified MWCNTs in acetone solution was investigated using an Olympus BX60 optical microscope (OM). Solid epoxy nanocomposites were prepared using the same curing procedure as previously reported.[8] The dispersion and degree of disentanglement of the F-MWCNTs was investigated using a Technai T20 computerized transmission electron microscope (TEM) operating at an accelerating voltage of 200 kV. The cured epoxy nanocomposite contained 1.1 wt % F-MWCNTs. TEM thin sections, with a thickness of about 100 nm, were prepared using a Reichert-Jung Ultracut E microtome with a diamond knife.

Rheological measurements were carried out using an ARES-G2 rotational rheometer (TA Instruments). The environmental conditions were maintained using a forced convection oven with dried air flow at constant rate. Temperature was monitored with a piezoelectric thermocouple mounted beneath the bottom fixture and was verified to be within ±0.1 °C of the reported temperature for all measurements. All measurements were carried out with parallel plate geometries (25 and 40 mm diameter, with a gap of 1.5−3 mm). To determine the role of loading history, measurements were carried out before and after the application of steady shear. Linear and nonlinear viscoelastic measurements were reproducible following steady shear, and the reported measurements are from representative presheared suspensions.

Small-amplitude oscillatory shear (SAOS) measurements were carried out within the linear viscoelastic region (LVR) of each suspension over a frequency range of ω = 0.01−100 rad/s. The LVR was determined from large-amplitude oscillatory shear (LAOS) measurements, which were carried out at a fixed angular frequency of ω = 10 rad/s and a strain amplitude of γ = 0.1−500%. Steady shear viscosity was measured with two separate sweeps to verify consistency of measurements. The first sweep was carried out by increasing the shear rate from $\dot{\gamma}$ = 10^{-3} to 100 s^{-1}. A second sweep was subsequently performed by decreasing $\dot{\gamma}$ over the same range. Up to 5 min was allowed to reach steady state viscosity during each measurement. Unless otherwise noted, the results of the two sweeps were nearly identical. The steady shear viscosity was also measured at constant shear rate over time to verify steady state was reached. The maximum shear rate was limited to $\dot{\gamma}$ = 100 s^{-1} to prevent ejection of material from the gap and prevent shear-induced heating of the samples. To confirm that wall slip was absent, the gap between parallel plates was varied between multiple measurements, and no change in linear viscoelastic or steady shear response was observed. Due to limitations in the resolution of the transducer, any measurements with stress near or smaller than ∼0.1 Pa were discarded. Machine inertia at high angular frequency was confirmed to be negligible below ω = 100 rad/s.

The behavior of the unfilled epoxy is Newtonian over the conditions reported here. The transducer resolution limited the measurement of the low-frequency elastic response of the epoxy and suspensions at low concentration. To determine the magnitude of elastic response, the frequency domain of the unfilled epoxy was measured at temperatures down to 10 °C, and shifted to T_{ref} = 25 °C using time−temperature superposition.

RESULTS

Functionalization of MWCNTs and Dispersion in Epoxy. Chemical oxidation with strong acids is a common method used to purify and disperse MWCNTs.[17,18] To achieve a suitable degree of dispersion, extensive treatment at elevated temperatures is usually required, which may compromise the

dx.doi.org/10.1021/jp4110272 | J. Phys. Chem. B 2014, 118, 362−371

structure and physical properties of the nanotubes. Here, the oxidative treatment was carried out under moderate conditions that have been previously reported to preserve the structural integrity and electrical properties of the MWCNTs.[10,18−21] The oxidized MWCNTs were functionalized by reaction with 4-nitroaniline in acetonitrile solvent (Figure 1). The dispersion

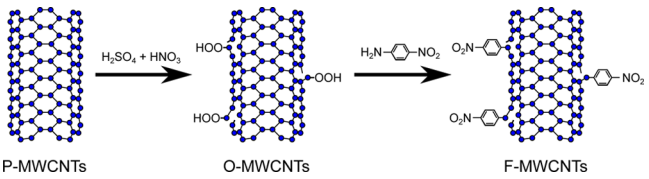

Figure 1. Schematic showing the functionalization route used in this work. Pristine MWCNTs (P-MWCNTs) are oxidized to introduce reactive sites along sidewalls. The oxidized MWCNTs (O-MWCNTs) are reacted with 4-nitroaniline in acetonitrile solution, which introduces nitrobenzene (NB) functionalities. The NB-functionalized MWCNTs are easily dispersed in acetone and other organic media as individual nanoparticles.

and stability of the MWCNTs in organic solvent are significantly improved by the functionalization reaction (Supporting Information). On the basis of visual and OM inspection, the F-MWCNTs appear to be homogeneously dispersed in acetone, and show no observable precipitation after several days. For the untreated MWCNTs, significant phase separation is observed minutes after sonication.

The functional groups were identified by comparing the IR absorption spectra of the F-MWCNTs with untreated MWCNTs using FTIR-ATR (Figure 2). The F-MWCNTs

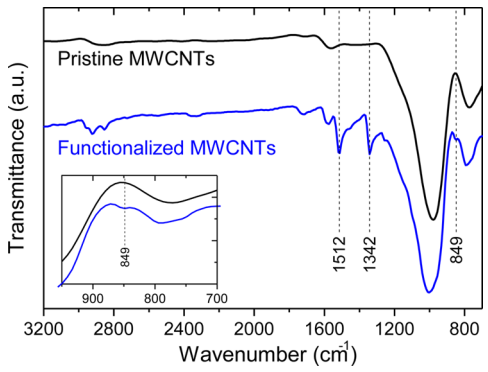

Figure 2. FTIR-ATR spectra of pristine MWCNTs and NB-functionalized MWCNTs.

show strong, distinct absorbance peaks at 1512 and 1342 cm^{-1} and a weaker peak at 849 cm^{-1}, which are consistent with the vibrational frequencies of the C−NO_2 group in nitrobenzene (NB).[22−24] The sharp peak at 1512 cm^{-1} is assigned to the asymmetric stretching of NO_2 and ring stretching of benzene.[25] The peaks at 1342 and 849 cm^{-1} are assigned to the symmetric stretching and scissoring motion of NO_2, and confirm the presence of NB functionalities.[24] The change in absorption spectra near 3000 and 1450 cm^{-1} is consistent with our prior report on oxidized MWCNTs prepared with identical treatment,[11] and indicates the presence of unreacted −COOH sites.

The concentration of functional groups was estimated using TGA (Supporting Information). The F-MWCNTs show much larger mass loss than the P-MWCNTs or O-MWCNTs at 800 °C in a N_2 environment, which confirms that a large concentration of functional groups is present. XPS measurements were also carried out and support the presence of a high concentration of chemically grafted NB groups on the F-MWCNTs (Supporting Information).

The F-MWCNTs were transferred to an epoxy matrix without any visible aggregation or change in dispersion state. Solid epoxy nanocomposites were prepared at 1.1 wt % and analyzed with TEM (Figure 3). The micrograph in Figure 3 is

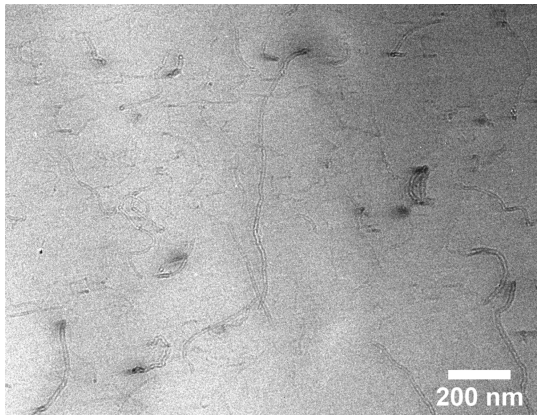

Figure 3. TEM of fully cured epoxy nanocomposite containing 1.1 wt % NB-functionalized MWCNTs.

representative of the observed dispersion state throughout the system. Previous studies found that untreated and oxidized MWCNTs are highly entangled and poorly dispersed on the individual level at similar concentrations.[8,11] The TEM micrographs show that the F-MWCNTs are individually dispersed and randomly distributed throughout the epoxy matrix, and show no evidence of increased defect concentration or reduction in nanotube length.

The above results show that the functionalization reaction introduces NB functionalities along the MWCNT sidewalls, and results in excellent dispersion and stability, even after long curing time in a low viscosity fluid (~4 h cure). Unfortunately, these tools provide only indirect characterization regarding the nature of interparticle interaction and mechanism of stability. Rheology is used as a more direct probe to investigate the microstructure and interactions of the dispersed MWCNTs.

Linear Viscoelasticity of Clustered MWCNTs. An initial series of investigations were carried out on the rheological response of untreated MWCNTs. P-MWCNTs were dispersed in acetone by brief sonication at room temperature. The epoxy was dissolved in the acetone/P-MWCNT mixture, and the mixture was slowly dried with a rotary evaporator. Suspensions of P-MWCNTs were prepared with mass fraction, c, varied over 4 decades, from 0.001 to 10 wt %. At low concentration, $c \approx$ 0.001− .09 wt %, the systems are visually homogeneous and settle over a period of a few minutes. OM studies show that the MWCNTs are clustered on the micrometer scale (Supporting Information). There is no discernible change in fluid rheology up to mass fraction, $c \sim$ 0.09 wt %. At $c \sim$ 0.1−0.2 wt %, large clumps become apparent throughout the fluid and strongly adhere to the walls of the containers. At ~2 wt %, the suspensions are weak gels and do not flow due to gravity alone. For these systems, the samples were removed from a flat-bottomed container using a razor blade and manually transferred to the parallel plates for rheological measurements. At 5 and 10 wt %, the suspensions were not deformed by

dx.doi.org/10.1021/jp4110272 | J. Phys. Chem. B 2014, 118, 362−371

vertical displacement of the transducer at room temperature with normal force up to the maximum load of the instrument, 2000 g. These suspensions are strong gels with an apparent bulk modulus. The gap was reduced by increasing the temperature to 120 °C and applying a combination of compressive axial force with steady shearing deformation. The qualitative trend of behavior is similar to earlier reports,[26] and shows that the nature of response observed here is an appropriate baseline for discussion of clustered structure.

The linear viscoelastic response of several representative P-MWCNT suspensions is shown in Figure 4. The storage modulus, G', is a measure of the ability of a material to store strain energy and recover shape following small amplitude oscillatory deformation, and corresponds to solid-like response. For relatively dilute systems, G' increases weakly with concentration, and is most significant at low frequency. At ~0.1−0.2 wt %, there is a plateau in G' in the limit of low frequency, which may be used to define the network modulus, G_0. As concentration increases, the power-law slope of G' progressively decreases, and the plateau region extends to higher frequency. The magnitude of G_0 increases weakly with concentration up to ~1 wt %. At higher concentration, G' is relatively independent of frequency over the experimental range and G_0 rapidly diverges with concentration. The divergence in elastic response is typical of a sol−gel transition.[27,28] The linear viscoelastic behavior is qualitatively identical to prior reports of both untreated and treated MWCNTs,[29−32] and of oxidized carbon nanofibers (CNFs).[33]

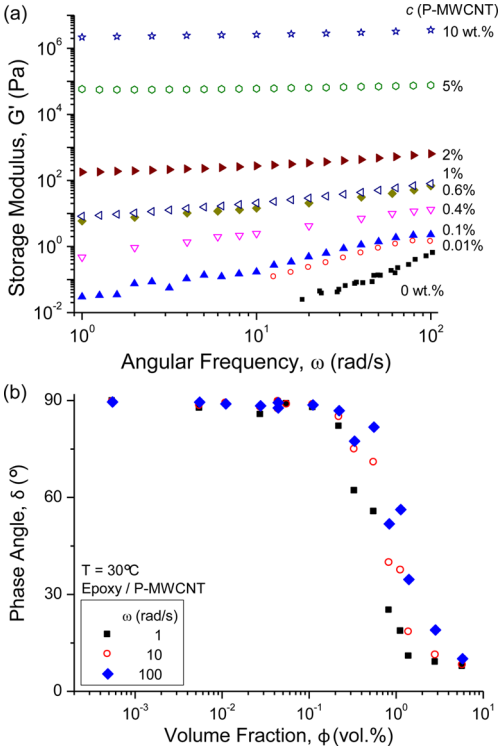

Figure 4. Linear viscoelasticity of clustered MWCNTs dispersed in epoxy. (a) Storage modulus, G', as a function of angular frequency, ω, for MWCNT suspensions with mass fraction, c, ranging from 0.01 to 10 wt %. (b) Phase angle, δ, as a function of volume fraction, ϕ, for measurements at angular frequencies of 1, 10, and 100 rad/s. Measurements carried out at 30 °C.

The transition behavior can be clearly observed from the change in phase angle, δ, with volume fraction, ϕ (Figure 4b). The phase angle is a characteristic measure of relative liquid-like or solid-like response, and ranges from 90° for an ideal Newtonian liquid to 0° for an ideal Hookean solid. The suspensions show predominantly Newtonian response up to $\phi \approx 0.1$ vol % (≈0.2 wt %). Above this limit, δ decreases sharply with concentration, and is most significantly reduced at low frequency. At the highest concentration, $\phi = 5.5$ vol %, $\delta \approx 10°$, independent of frequency.

The linear viscoelasticity of MWCNT suspensions has been reported for a range of systems considering different treatment methods, and for Newtonian and non-Newtonian media.[5,29−32,34−38] The prior reports are consistent with the trends reported in Figure 4. The most distinctive feature of the linear viscoelastic response is the low-frequency plateau in G', which is observed here for P-MWCNT loadings of ~0.2 wt % and higher. This behavior indicates that the suspension is unable to relax and recover a liquid-like response on the experimental time scale, $\tau \sim 1/\omega$.

Linear Viscoelasticity of Disentangled MWCNTs. Suspensions containing F-MWCNTs were prepared at concentrations of 0.1, 0.5, and 1.0 wt %. The linear viscoelastic response of the F-MWCNT suspensions is shown in Figure 5 and summarized in Table 1. Each of the systems shows a similar response, which indicates that there is no transition in microstructure with concentration. The magnitude of G' and

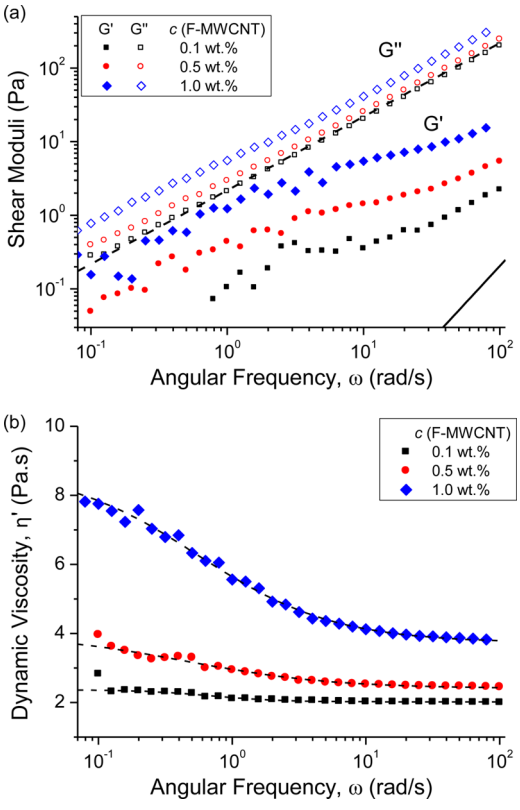

Figure 5. Linear viscoelasticity of disentangled MWCNT suspensions. (a) Storage modulus, G' (filled), and loss modulus, G'' (unfilled), shown as functions of angular frequency, ω, for 0.1, 0.5, and 1.0 wt % F-MWCNT in epoxy. (b) Dynamic viscosity, $\eta' = G''/\omega$, plotted as a function of angular frequency. The lines in part a show the response of unfilled epoxy fluid. The dotted lines in part b were fitted to the Cross equation, eq 1. Measurements carried out at $T = 30$ °C.

dx.doi.org/10.1021/jp4110272 | J. Phys. Chem. B 2014, 118, 362−371

Table 1. Summary of Linear Viscoelastic Behavior for NB-Functionalized MWCNTs in Epoxy[a]

	c (wt % F-MWCNT)		
	0.1	0.5	1.0
α (low ω)	0.65	0.79	0.86
α (high ω)	0.86	0.83	0.59
η_0' (Pa·s)	4.2	8.5	13.4
η_∞' (Pa·s)	2.1	2.5	3.4
λ (s)	104.7	92.5	14.8
n	0.50	0.45	0.48

[a] c is the mass fraction; α is the power-law slope for frequency dependence of G' ($G' \sim \omega^\alpha$) in a specified frequency range. Dynamic viscosity curves fit using the Cross equation (eq 1): η_0' and η_∞' are zero-frequency and infinite-frequency dynamic viscosities, λ is the time constant, and n is the degree of shear thinning. Measurements carried out at T = 30 °C on presheared samples.

G'' increases with concentration, and there appear to be three frequency domains. The scaling of elastic response may be expressed by $G' \sim \omega^\alpha$, where α is the power-law exponent. In the limit of low frequency, α increases with concentration, and at c = 1 wt % F-MWCNT, G' is nearly linear with frequency. At intermediate frequency, there is a narrow region with weaker frequency dependence, and in the limit of high frequency, the slope increases again. It is difficult to differentiate between the regions due to the noise in G' for the lower concentration systems, but it is clear that the transition between the low frequency and intermediate frequency regions, designated ω_c, is not strongly dependent on concentration (Supporting Information).

Due to the small stresses at low frequency for the 0.1 and 0.5 wt % F-MWCNT systems, the trend of increasing α with c is not regarded as significant. At high frequency, the contribution of the unfilled epoxy matrix, which follows $G' \sim \omega^2$, will also contribute to larger α. Due to these limitations, the significance of the power-law exponents will be discussed on the basis of only the 1 wt % system.

At high and low frequency, $G'' \sim \omega$, for each system, which indicates that the limiting dynamic viscosity, $\eta'(\omega) = G''/\omega$, is constant. The zero-frequency and infinite-frequency dynamic viscosities are defined as $\eta_0' = \lim_{\omega\to 0}\eta'$ and $\eta_\infty' = \lim_{\omega\to\infty}\eta'$. Each of the F-MWCNT systems show a clear transition to a high frequency plateau region with constant dynamic viscosity η_∞'. There also appears to be a low-frequency region for each concentration. However, the scatter in $\eta' = G''/\omega$ is significantly amplified at low frequency due to small variations in G'', and it is difficult to clearly define η_0'. The magnitudes of limiting dynamic viscosities were quantified using the Cross equation,[39] which is given by

$$\eta' = \eta_\infty' + \frac{\eta_0' - \eta_\infty'}{1 + (\lambda\omega)^n} \quad (1)$$

where λ is a characteristic time corresponding to the midpoint of the frequency-thinning transition and n is the power-law exponent (Table 1).

The shear moduli, G' and G'', are useful descriptors for the magnitude and scaling behavior corresponding to solid-like and liquid-like response, respectively. However, both parameters are derived from the magnitude of complex modulus, $|G^*|$, and phase angle, δ, and are therefore inter-related. As a result, it is challenging to clearly determine subtle changes in relaxation behavior based on these quantities alone. Van Gurp and Palmen (vGP)[40] showed that plotting $\delta = f(|G^*|)$ provides a temperature-independent representation to compare between sets of data. The original approach was proposed for validation of the application of time−temperature superposition, and has since been used to identify subtle relaxation processes in various complex fluids and polymers.[41−44]

The vGP representation of linear viscoelasticity for the F-MWCNT systems is shown in Figure 6. High values of $|G^*|$

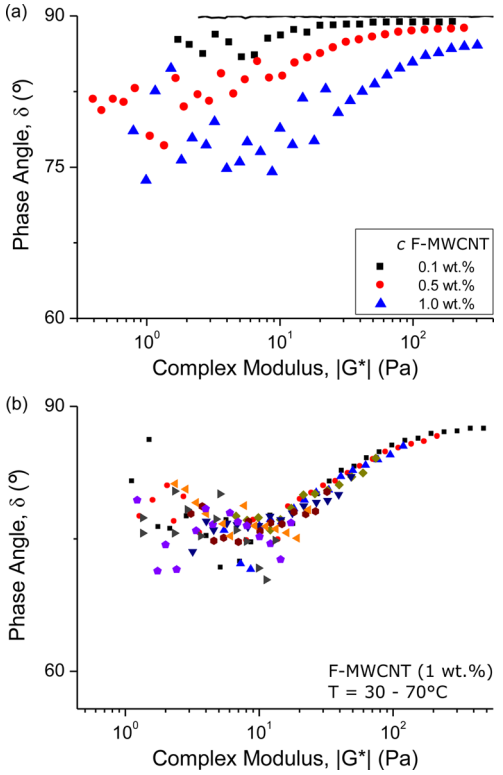

Figure 6. Relaxation behavior of disentangled MWCNT suspensions. (a) Phase angle, δ, plotted as a function of the magnitude of complex modulus, $|G^*|$ (vGP plot), for 0.1, 0.5, and 1.0 wt % F-MWCNT. The solid line corresponds to unfilled epoxy matrix. (b) vGP plot for 1.0 wt % F-MWCNT showing measurements carried out from 30 to 70 °C. No shift factor was used to account for temperature effects.

correspond to high frequency and low temperature measurements, and reflect localized, short-range processes dominated by hydrodynamic interactions. As $|G^*|$ decreases, the relaxation behavior is determined by slower, longer-range processes. For the F-MWCNT suspensions, the curves are similar at all concentrations. There is a plateau region of $\delta \approx 90°$ at high $|G^*|$ and a progressive decrease in δ on longer time scales. As concentration increases, there is a shift in the curve to higher $|G^*|$ and the maximum in δ is decreased. At 1 wt %, there is a minimum at $\delta_n \approx 75°$, which corresponds to a transition in relaxation behavior to viscous flow. As the concentration decreases, the minimum in phase angle approaches 90°, which agrees with recent observations on the rheology of model suspensions containing individually dispersed nanoplatelets.[43,44] There is some noise in this value due to the low magnitude of oscillation stress at the corresponding low frequency.

Additional measurements were carried out at higher temperatures and showed similar δ_n (Figure 6b), which support the existence of a minima rather than a plateau. The relaxation

dx.doi.org/10.1021/jp4110272 | J. Phys. Chem. B 2014, 118, 362−371

transition to viscous flow behavior at low frequency confirms that there is no long-range microstructure associated with the MWCNT phase. In contrast, the P-MWCNT systems at concentrations above the transition concentration show a sharp shift in vGP behavior to higher $|G^*|$ and lower δ, and show no change in slope at lower $|G^*|$. This corresponds to a progressive increase in solid-like response on longer time scales, and shows the dominant role of elastic stresses within the clustered network. This observation fits with the proposed mechanism for elastic instabilities suggested by Lin-Gibson et al.[34] The robustness of this claim is considered in detail below.

In the suspensions containing P-MWCNTs at low concentration, there is a weak increase in storage modulus and a negligible change in loss modulus with concentration. At $\phi \approx 0.2$ vol %, there is a divergence in G', and at higher concentration, it follows $G' \sim \phi^4$. The loss modulus, G'', diverges at slightly higher concentration, $\phi \approx 0.6$ vol %, and follows $G'' \sim \phi^3$. The significance of the power-law exponents and related percolation-type behavior has been discussed at length in prior works and will not be considered here.[31] The F-MWCNT systems do not show the same divergent behavior (Supporting Information).

The change in linear viscoelastic response due to disentanglement was further investigated by carrying out measurements over a range of temperatures (Figure 7). Time−temperature superposition was used by independently determining time and stress shift factors, a_T and b_T.[45] The significance of the shift factors is discussed below. The storage modulus of the suspension containing untreated MWCNTs is largest, and shows clearly defined low-frequency plateau and high-frequency scaling of $\omega^{0.75}$. The oxidized MWCNTs show much better dispersion but retain a plateau in G' at low frequency, which is indicative of a spanning network of MWCNT aggregates. Similar behavior in CNF suspensions after chemical oxidation was reported by Xu et al.[33]

For the F-MWCNTs, the measurements obtained over a range of temperatures are consistent with behavior at room temperature, and confirm that there is a distinct change in the nature of relaxation due to disentanglement. The high-frequency scaling behavior is independent of treatment, which suggests that the measurements reflect the behavior of the individual MWCNTs. For perfectly rigid rod-like particles, there is a plateau in G' at high frequency.[46] Deviations in scaling are generally attributed to internal modes of flexibility.[47]

The change in phase angle, δ, with the magnitude of complex modulus, $|G^*|$, is a sensitive tool to show changes in relaxation behavior,[40−42,48] and clearly shows that the behavior of the NB-functionalized MWCNTs is distinct from the effect of chemical oxidation alone (Figure 7b). An additional system is included where the MWCNTs are oxidized and functionalized with sulfanilamide, MWCNT-SAA. The functionalization route is identical to that previously described by Warren et al.,[15] and results in a significantly improved dispersion state. However, there is apparently no significant change in the nature of interparticle interaction for this system. The distinct response observed here, in comparison with the nearly universal behavior reported in prior works on CNTs with and without surface treatment, suggests that the functionalization route suppresses the attractive interactions between MWCNTs. Klingenberg and colleagues reported that, even in the absence of attractive interaction, fiber-like particles tend to aggregate into flocculated structures due to interfacial friction alone.[49−53] On the basis of the results presented here, the NB functionalities might also

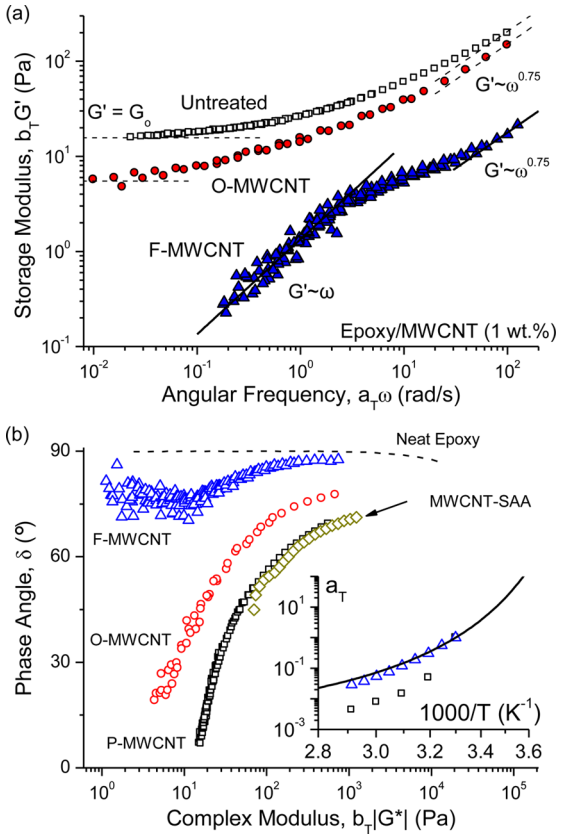

Figure 7. (a) Linear viscoelastic master curves for suspensions containing 1 wt % MWCNT with different treatments. The solid line shows limited scaling of disentangled F-MWCNT suspensions at high frequency, $G' \sim \omega^{0.75}$, and low frequency, $G' \sim \omega$. Dotted lines show limited scaling of untreated and oxidized MWCNT suspensions at high and low frequencies. (b) Corresponding vGP plots for the same systems. The dotted line in part b shows the response of unfilled epoxy. The inset is the horizontal shift factor for time−temperature superposition, a_T. The solid line is the WLF fit to unfilled epoxy. The symbols in the inset are the same as those in part b.

contribute to a weak repulsive force that limits the role of friction in stabilizing flocs. Detailed analysis of the nature of interaction between the NB functionalities and the suspending matrix is not considered here but may provide additional insights into the observed stability and relaxation behavior reported here.

For the unfilled epoxy and F-MWCNT systems, no stress shift factor, b_T, was needed to obtain time−temperature superposition. It is possible that the fit could be improved at lower frequency with the additional shift factor to account for the change in matrix density (Figure 6b),[45] but the fit was acceptable with b_T fixed at 1 for temperatures between 30 and 70 °C. For the untreated and oxidized MWCNTs, a large stress shift factor was required, which suggests the presence of an additional temperature-dependent mechanism. The observed increase in elastic response with temperature is consistent with the "mechanical flocculation" mechanism described by Schmid et al. for fiber suspensions.[50] The magnitude of the time shift factor is also larger for the untreated MWCNTs. For the F-MWCNTs, a_T is nearly identical to the unfilled matrix (Figure 7b).

Steady Shear Response. The steady shear response of the F-MWCNT suspensions is shown in Figure 8. The parameters describing the flow curves were determined with eq 1, where η_0'

dx.doi.org/10.1021/jp4110272 | J. Phys. Chem. B 2014, 118, 362−371

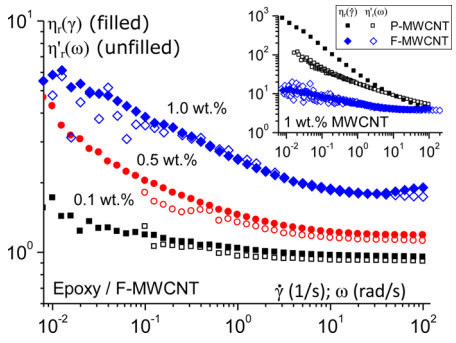

Figure 8. Cox–Merz plot for F-MWCNT suspensions. Relative steady shear viscosity, $\eta_r(\dot{\gamma})$ (filled symbols), and dynamic viscosity, $\eta'_r(\omega)$ (unfilled symbols), of the F-MWCNT suspensions in epoxy plotted as functions of shear rate, $\dot{\gamma}$, and angular frequency, ω, respectively. The inset shows the Cox–Merz plot of epoxy containing 1 wt % P-MWCNT and F-MWCNT.

and η'_∞ are replaced by zero and infinite shear rate viscosities, η_0 and η_∞, respectively, and angular frequency, ω, is replaced by shear rate, $\dot{\gamma}$. The steady shear parameters are summarized in Table 2. The shear viscosity, $\eta(\dot{\gamma})$, and dynamic viscosity, $\eta'(\omega)$, are in excellent agreement for the suspensions at 0.1 and 0.5 wt % at all shear rates. The agreement between viscosity measurements obtained under small amplitude oscillatory deformation and steady shearing is commonly referred to as the Cox–Merz law. The empirical relationship indicates that the relationships between structure and rate are the same for the weakly and strongly perturbed microstructure, and shows that there is no significant breakdown or permanent change in microstructure due to large shearing forces.

Table 2. Summary of Rate-Dependent Parameters for Steady Shear Viscosity of NB-Functionalized MWCNTs Dispersed in Epoxy[a]

c (wt %)	η_0 (Pa·s)	η_∞ (Pa·s)	λ (s)	n
0.1	4.2	2.1	104.7	0.46
0.5	11.2	2.5	92.5	0.58
1.0	16.3	3.4	20.6	0.55

[a]Parameters determined by fitting measurements to the Cross equation (eq 1): η_0 and η_∞ are zero shear rate and infinite shear rate shear viscosities. Measurements carried out at T = 30 °C on presheared samples.

The steady shear responses of the P-MWCNT and F-MWCNT systems at 1 wt % are shown in the inset of Figure 8. The dynamic viscosities from the linear viscoelastic master curves are also shown. The P-MWCNT system shows nearly identical viscosity to the disentangled system at high shear rates. As shear rate decreases, the difference between the untreated and disentangled systems diverges significantly. The behavior of the untreated MWCNTs is consistent with a flocculated microstructure. The number of particles confined in the floc structure is determined by the balance between attractive forces and hydrodynamic stresses.[54] The agreement at high shear rate supports previous claims that the MWCNT flocs are broken down to the individual particle level at high shear rates.[31]

For the 1 wt % F-MWCNT system, the Cox–Merz rule is followed for all measurements except at high shear rate. During steady shear, the system shows weak shear thickening behavior. The behavior was observed over consecutive measurements, independent of the direction of shear rate sweeps, and with shear rate ramps. To probe the time scale associated with the transition, additional measurements were carried out at higher temperatures (Figure 9). The shear rate at the thickening transition, $\dot{\gamma}_c$, increases with temperature, and is observable up to 40 °C. At higher temperatures, there is no change in behavior, but the viscosity minimum prior to thickening is outside of the experimental range. The measurements were reduced using the rotary Peclet number, $Pe = \dot{\gamma}/D_r$. The rotary diffusion coefficient, D_r, for high aspect ratio, rod-like particles is given by

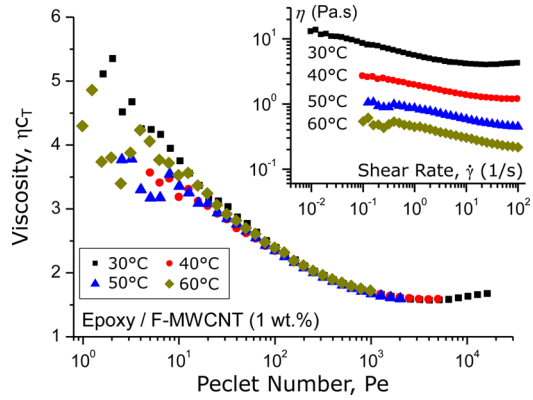

Figure 9. Shear thickening of disentangled MWCNTs in epoxy precursor at 1.0 wt % concentration. Shear viscosity shown as a function of Peclet number, $Pe = \dot{\gamma}/D_r$, where D_r is the rotary diffusion coefficient (eq 2). The vertical shift factor, c_T, is on the order of $1/\eta_s$. The inset shows raw measurements of viscosity as a function of shear rate at different temperatures.

$$D_r = 3kT[\ln(r_p) - 0.8]/\pi\eta_s L^3 \quad (2)$$

where K is Boltzmann's constant, T is the absolute temperature, $r_p = L/d$ is the aspect ratio, L and d are the length and diameter of the rod, and η_s is the viscosity of the unfilled solvent. For the MWCNTs used here, $L \sim 1$ μm, and $r_p \sim 100$, which gives $D_r \approx 0.007$ s^{-1} for T = 30 °C. Scaling by D_r provides excellent superposition of the individual measurements carried out at different temperatures.

DISCUSSION

The rheology and viscoelasticity of MWCNTs in epoxy have been investigated in a number of previous works. However, to our knowledge, there are no previous reports that have clearly probed the elastic response associated with motion of individually dispersed MWCNTs in epoxy. The objective of this discussion is to consider the molecular-scale origin of viscoelastic response and steady shear behavior for the suspensions containing disentangled MWCNTs in epoxy.

In the absence of significant colloidal interaction, the rate-dependent properties of suspensions containing solid particles are predominantly governed by the balance between Brownian motion and hydrodynamic stresses. For nonspherical particles, Brownian motion acts to randomize the position and orientation of the particles, which results in measurements that are independent of initial loading conditions. Brownian motion also introduces rotary diffusional torques due to the distribution of particle orientations in the velocity field, which results in additional viscous and elastic stresses that scale linearly with the rate of deformation.[55]

dx.doi.org/10.1021/jp4110272 | J. Phys. Chem. B 2014, 118, 362–371

In the limit of zero frequency, both Brownian motion and hydrodynamic interactions are present and make distinct contributions to elastic and viscous components of response. In the limit of infinite frequency, the time scale of deformation is too rapid for significant Brownian motion to occur, and the elastic contribution vanishes. For an infinitely dilute suspension of rod-like macromolecules, the time scale for the transition between regions is $\tau = 1/6D_r$, which is the time required for an isolated rod to rotate end-over-end in a shearing field. Assuming the MWCNTs have $L = 1$ μm and $r_p = 100$, $\tau \approx$ 24 s at 30 °C, and the expected transition frequency is $\omega_c \sim$ 0.04 rad/s. The transition observed in the F-MWCNT systems is significantly higher, $\omega_c \approx 2.6$ rad/s.

The discrepancy may be due, in part, to the potential change in shape and size of the MWCNTs following chemical modification. For a fixed diameter of 10 nm and $r_p = 30$, $\omega_c \approx 1.1$ rad/s. The TEM evidence in Figure 2 suggests that there is not a significant decrease in MWCNT length, and our prior works have found that similar treatment does not introduce detectable damage to the nanotube structure.[10,11,19−21,56,57] However, due to the large aspect ratio and nonuniform length distribution of the MWCNTs, it is challenging to explicitly verify the distribution of fiber lengths. The transition frequency may also be increased due to hydrodynamic interaction between fibers, which increases the rate of fiber rotation out of the flow direction and may reduce τ.[58,59]

As the concentration of F-MWCNT increases, there is no significant change in transition frequency (Figure 4). The concentration dependence of polymers is typically modeled on the basis of an assumption that neighbors inhibit rotational diffusivity, which results in an entanglement transition and a drastic increase in relaxation time.[60,61] The lack of concentration dependence is strong evidence there is no entanglement present for the F-MWCNT suspensions. The relaxation behavior of the MWCNTs in epoxy may be viewed as intermediate between the behavior of rod-like polymers (molecular scale) and semiflexible fibers (micrometer scale). Further investigations that employ molecular modeling of this system will be useful to identify specific features regarding the rotational and translational dynamics of the individual MWCNTs in suspension.

The final feature that warrants consideration is the observed shear thickening in the 1.0 wt % F-MWCNT system at high shear rate. Shear thickening is generally associated with a system-wide instability, such as the disruption of a layered structure, or the hydrodynamic compression of deformable spheres.[62,63] Here, the MWCNTs are individually dispersed and disentangled, and there is no evidence to suggest any mesoscale structure or liquid crystalline organization. At high shear rate, the degree of order should be highest, and any interaction between neighboring MWCNTs will be minimized. One possible explanation to account for the thickening transition is a change in the shape of the MWCNTs due to shear-induced stresses. The relevant shear rate for deformation of an individual MWCNT during simple shearing may be estimated from the dimensionless bending stiffness proposed by Forgacs and Mason.[64,65] Assuming that the suspended MWCNTs are extended fibers, the dimensionless bending stiffness is given by

$$\mathrm{BS} = E_Y \pi / \eta_s \dot{\gamma} r_p^{\,4} \qquad (3)$$

where E_Y is the Young's modulus. For BS $\ll$ 1, the rigidity of the fibers is less than the magnitude of viscous shear stresses, and the fibers will tend to buckle due to compressional stresses experienced during steady shear. Here, the Young's modulus of the CVD-grown MWCNTs is estimated to be on the order of 50 GPa.[66] For a suspension of MWCNTs with uniform aspect ratio of $r_p = 100$, the dimensionless bending stiffness is ∼7 at T = 30 °C and $\dot{\gamma} = 100$ s^{-1}. This shows that the viscous stresses are of an appropriate magnitude to account for the deformation of the MWCNTs during shearing. If we assume that the transition is associated with the longest MWCNTs, which disrupt the locally organized domains after deforming, then the bending criterion given by eq 3 provides a reasonable agreement with the observed behavior. From eq 3, it is also apparent that the bending stiffness will increase with temperature, due to the decrease in viscosity of the matrix, which is consistent with the observations. The deformation of the MWCNTs above a critical shear rate will also alter the period of rotation for the individual particles, and modify the distribution of orbit constants. As a result, the microstructure in the vicinity of the particle will be significantly distorted. To our knowledge, this behavior has not been previously reported for suspensions of MWCNTs, or for the more general case of fiber-like particles. More detailed modeling efforts may provide further insight into the nature of the observed shear thickening transition, particularly the role of hydrodynamic interactions, which are responsible for discontinuous shear thickening in suspensions of monodisperse, concentrated spherical particles.

The rheological results presented here show that the functionalization approach used to obtain disentangled MWCNTs results in a stable structure with no flocculation on long time periods. The similarity in high frequency measurements is indirect evidence that there is no significant damage or change in shape and length of the MWCNTs following chemical treatment. In many applications, unique properties have been reported due to the formation of a controlled MWCNT aggregate structure.[8,9,67,68] In these cases, an individual, stable dispersion may not necessarily be desired. However, if the MWCNTs are able to modify the properties of the surrounding matrix, an individually dispersed microstructure may be preferable for maximum effect at low concentration.[10,11,57] For fundamental studies, the individual structure also allows distinction between clustered and individual MWCNTs to be determined.

CONCLUSIONS

This work has investigated the evolution of rheological and viscoelastic responses of clustered and disentangled MWCNTs dispersed in a stable, non-reactive Newtonian epoxy matrix. The rheological behavior of the clustered MWCNTs showed strong rate-dependent behavior. The development of linear viscoelastic and steady shear response in the suspension containing individually dispersed, functionalized MWCNTs in epoxy was significantly suppressed, and characteristic Brownian relaxation behavior was observed at low frequency. Characteristic features of the disentangled MWCNTs in epoxy were a lack of low-frequency plateau in storage modulus and shear thickening at high shear rate. The rheological behavior of the disentangled MWCNTs in epoxy is in agreement with continuum-level predictions based on the motion of individual, semiflexible fibers under shearing flows.

■ ASSOCIATED CONTENT

Supporting Information

OM and TEM showing dispersion of P-MWCNTs and F-MWCNTs in organic solvent; TGA of MWCNTs prepared with different treatments; details of the storage modulus as a function of angular frequency for F-MWCNT suspensions at different concentrations; and concentration dependence of storage and loss modulus for P-MWCNT and F-MWCNT suspensions. This material is available free of charge via the Internet at http://pubs.acs.org.

■ AUTHOR INFORMATION

Corresponding Author

*E-mail: hjsue@tamu.edu. Phone: (979)-845-3081.

Author Contributions

§These authors contributed equally.

Notes

The authors declare no competing financial interest.

■ ACKNOWLEDGMENTS

The authors acknowledge partial financial support by KANEKA Corporation. Haiqing Yao and Spencer Hawkins are acknowledged for assistance in sample preparation and for helpful discussion throughout the course of this work.

■ REFERENCES

(1) Salvetat, J.-P.; Bonard, J.-M.; Thomson, N.; Kulik, A.; Forro, L.; Benoit, W.; Zuppiroli, L. Mechanical Properties of Carbon Nanotubes. *Appl. Phys. A: Mater. Sci. Process.* **1999**, *69*, 255−260.

(2) Che, J.; Cagin, T.; Goddard, W. A., III. Thermal Conductivity of Carbon Nanotubes. *Nanotechnology* **2000**, *11*, 65−69.

(3) Berber, S.; Kwon, Y.-K.; Tomanek, D. Unusually High Thermal Conductivity of Carbon Nanotubes. *Phys. Rev. Lett.* **2000**, *84*, 4613.

(4) Bauhofer, W.; Schulz, S.; Eken, A.; Skipa, T.; Lellinger, D.; Alig, I.; Tozzi, E.; Klingenberg, D. Shear-Controlled Electrical Conductivity of Carbon Nanotubes Networks Suspended in Low and High Molecular Weight Liquids. *Polymer* **2010**, *51*, 5024−5027.

(5) Alig, I.; Skipa, T.; Lellinger, D.; Pötschke, P. Destruction and Formation of a Carbon Nanotube Network in Polymer Melts: Rheology and Conductivity Spectroscopy. *Polymer* **2008**, *49*, 3524−3532.

(6) Skipa, T.; Lellinger, D.; Saphiannikova, M.; Alig, I. Shear-Stimulated Formation of Multi-Wall Carbon Nanotube Networks in Polymer Melts. *Phys. Status Solidi B* **2009**, *246*, 2453−2456.

(7) Skipa, T.; Lellinger, D.; Böhm, W.; Saphiannikova, M.; Alig, I. Influence of Shear Deformation on Carbon Nanotube Networks in Polycarbonate Melts: Interplay between Build-up and Destruction of Agglomerates. *Polymer* **2010**, *51*, 201−210.

(8) White, K. L.; Sue, H.-J. Electrical Conductivity and Fracture Behavior of Epoxy/Polyamide-12/Multiwalled Carbon Nanotube Composites. *Polym. Eng. Sci.* **2011**, *51*, 2245−2253.

(9) White, K. L.; Sue, H.-J. Delamination Toughness of Fiber Reinforced Composites Containing a Carbon Nanotube/Polyamide-12 Epoxy Thin Film Interlayer. *Polymer* **2011**, *53*, 37−42.

(10) White, K. L.; Shuai, M.; Zhang, X.; Sue, H.-J.; Nishimura, R. Electrical Conductivity of Well-Exfoliated Single-Walled Carbon Nanotubes. *Carbon* **2011**, *49*, 5124−5131.

(11) Chu, C. C.; White, K. L.; Liu, P.; Zhang, X.; Sue, H.-J. Electrical Conductivity and Thermal Stability of Polypropylene Containing Well-Dispersed Multi-Walled Carbon Nanotubes Disentangled with Exfoliated Nanoplatelets. *Carbon* **2012**, *50*, 4711−4721.

(12) Sue, H.-J.; Garcia-Meitin, E.; Pickelman, D.; Yang, P. Optimization of Mode-I Fracture Toughness of High-Performance Epoxies by Using Designed Core-Shell Rubber Particles. In *Toughened Plastics I: Science and Engineering*; Riew, C. K., Kinloch, A. J., Eds.; ACS Publications: Washington, DC, 1993; Vol. *233*, pp 259−292.

(13) Vaia, R. A.; Maguire, J. F. Polymer Nanocomposites with Prescribed Morphology: Going Beyond Nanoparticle-Filled Polymers. *Chem. Mater.* **2007**, *19*, 2736−2751.

(14) Ganguli, S.; Roy, A. K.; Anderson, D. P. Improved Thermal Conductivity for Chemically Functionalized Exfoliated Graphite/Epoxy Composites. *Carbon* **2008**, *46*, 806−817.

(15) Warren, G. L.; Sun, L.; Hadjiev, V. G.; Davis, D.; Lagoudas, D.; Sue, H. J. B-Staged Epoxy/Single-Walled Carbon Nanotube Nanocomposite Thin Films for Composite Reinforcement. *J. Appl. Polym. Sci.* **2009**, *112*, 290−298.

(16) Sun, L.; Warren, G. L.; Sue, H.-J. Partially Cured Epoxy/SWCNT Thin Films for the Reinforcement of Vacuum-Assisted Resin-Transfer-Molded Composites. *Carbon* **2010**, *48*, 2364−2367.

(17) Esumi, K.; Ishigami, M.; Nakajima, A.; Sawada, K.; Honda, H. Chemical Treatment of Carbon Nanotubes. *Carbon* **1996**, *34*, 279−281.

(18) Datsyuk, V.; Kalyva, M.; Papagelis, K.; Parthenios, J.; Tasis, D.; Siokou, A.; Kallitsis, I.; Galiotis, C. Chemical Oxidation of Multiwalled Carbon Nanotubes. *Carbon* **2008**, *46*, 833−840.

(19) Sun, D.; Everett, W. N.; Chu, C. C.; Sue, H.-J. Single-Walled Carbon Nanotube Dispersion with Electrostatically Tethered Nanoplatelets. *Small* **2009**, *5*, 2692−2697.

(20) Zhang, X.; Sue, H. J.; Nishimura, R. Electrostatically Controlled Isolation of Debundled Single-Walled Carbon Nanotubes from Nanoplatelet Dispersant. *J. Mater. Chem.* **2012**, *22*, 6156−6164.

(21) Zhang, X.; Sue, H.-J.; Nishimura, R. Acid-Mediated Isolation of Individually Dispersed SWCNTs from Electrostatically Tethered Nanoplatelet Dispersants. *Carbon* **2013**, *56*, 374−382.

(22) Kuwae, A.; Machida, K. Vibrational Spectra of Nitrobenzene-D_0, -*P-D* and -D_5 and Normal Vibrations of Nitrobenzene. *Spectrochim. Acta, Part A* **1979**, *35*, 27−33.

(23) Laposa, J. Vibrational Spectra of Nitrobenzene-D_5. *Spectrochim. Acta, Part A* **1979**, *35*, 65−71.

(24) Varsanyi, G.; Holly, S.; Imre, L. Some Characteristic Vibration Patterns of the Organic Nitro Group. *Spectrochim. Acta, Part A* **1967**, *23*, 1205−1210.

(25) Clarkson, J.; Ewen Smith, W. A DFT Analysis of the Vibrational Spectra of Nitrobenzene. *J. Mol. Struct.* **2003**, *655*, 413−422.

(26) Shaffer, M. S.; Fan, X.; Windle, A. Dispersion and Packing of Carbon Nanotubes. *Carbon* **1998**, *36*, 1603−1612.

(27) Winter, H. H.; Chambon, F. Analysis of Linear Viscoelasticity of a Crosslinking Polymer at the Gel Point. *J. Rheol.* **1986**, *30*, 367−382.

(28) Winter, H. H.; Mours, M. Rheology of Polymers near Liquid-Solid Transitions. *Adv. Polym. Sci.* **1997**, *134*, 165−234.

(29) Hobbie, E.; Fry, D. Nonequilibrium Phase Diagram of Sticky Nanotube Suspensions. *Phys. Rev. Lett.* **2006**, *97*, 036101.

(30) Hobbie, E.; Fry, D. Rheology of Concentrated Carbon Nanotube Suspensions. *J. Chem. Phys.* **2007**, *126*, 124907.

(31) Hobbie, E. K. Shear Rheology of Carbon Nanotube Suspensions. *Rheol. Acta* **2010**, *49*, 323−334.

(32) Rahatekar, S. S.; Koziol, K. K.; Kline, S. R.; Hobbie, E. K.; Gilman, J. W.; Windle, A. H. Length-Dependent Mechanics of Carbon-Nanotube Networks. *Adv. Mater.* **2009**, *21*, 874−878.

(33) Xu, J.; Chatterjee, S.; Koelling, K. W.; Wang, Y.; Bechtel, S. E. Shear and Extensional Rheology of Carbon Nanofiber Suspensions. *Rheol. Acta* **2005**, *44*, 537−562.

(34) Lin-Gibson, S.; Pathak, J.; Grulke, E.; Wang, H.; Hobbie, E. Elastic Flow Instability in Nanotube Suspensions. *Phys. Rev. Lett.* **2004**, *92*, 048302−048301−048304.

(35) Fry, D.; Langhorst, B.; Kim, H.; Grulke, E.; Wang, H.; Hobbie, E. K. Anisotropy of Sheared Carbon-Nanotube Suspensions. *Phys. Rev. Lett.* **2005**, *95*, 038304.

(36) Wang, H.; Christopherson, G.; Xu, Z.; Porcar, L.; Ho, D.; Fry, D.; Hobbie, E. Shear-SANS Study of Single-Walled Carbon Nanotube Suspensions. *Chem. Phys. Lett.* **2005**, *416*, 182−186.

(37) Fry, D.; Langhorst, B.; Wang, H.; Becker, M.; Bauer, B.; Grulke, E.; Hobbie, E. Rheo-Optical Studies of Carbon Nanotube Suspensions. *J. Chem. Phys.* **2006**, *124*, 054703.
(38) Ureña-Benavides, E. E.; Kayatin, M. J.; Davis, V. A. Dispersion and Rheology of Multiwalled Carbon Nanotubes in Unsaturated Polyester Resin. *Macromolecules* **2013**, *46*, 1642−1650.
(39) Cross, M. M. Rheology of Non-Newtonian Fluids: A New Flow Equation for Pseudoplastic Systems. *J. Colloid Sci.* **1965**, *20*, 417−437.
(40) van Gurp, M.; Palmen, J. Time-Temperature Superposition for Polymeric Blends. *Rheol. Bull.* **1998**, *67*, 5−8.
(41) Trinkle, S.; Friedrich, C. Van Gurp-Palmen-Plot: A Way to Characterize Polydispersity of Linear Polymers. *Rheol. Acta* **2001**, *40*, 322−328.
(42) Trinkle, S.; Walter, P.; Friedrich, C. Van Gurp-Palmen Plot II−Classification of Long Chain Branched Polymers by Their Topology. *Rheol. Acta* **2002**, *41*, 103−113.
(43) White, K. L.; Wong, M.; Li, P.; Miyamoto, M.; Sue, H.-J. Rheology of Smectic Liquid Crystals Formed from Exfoliated Nanoplatelets Dispersed in Uncured Epoxy Fluid. *Langmuir*, submitted for publication.
(44) White, K. L.; Li, P.; Yao, H.; Nishimura, R.; Sue, H.-J., Effect of Surface Modifier on Flow Properties of Epoxy Suspensions Containing Model Plate-Like Nanoparticles. *J. Colloid Interface Sci.*, submitted for publication.
(45) Dealy, J.; Plazek, D. Time-Temperature Superposition—a Users Guide. *Rheol. Bull.* **2009**, *78*, 16−31.
(46) Nemoto, N.; Schrag, J. L.; Ferry, J. D.; Fulton, R. W. Infinite-Dilution Viscoelastic Properties of Tobacco Mosaic Virus. *Biopolymers* **1975**, *14*, 409−417.
(47) Warren, T. C.; Schrag, J. L.; Ferry, J. D. Infinite-Dilution Viscoelastic Properties of Poly-Γ-Benzyl-L-Glutamate in Helicogenic Solvents. *Biopolymers* **1973**, *12*, 1905−1915.
(48) White, K. L.; Jin, L.; Ferrer, N.; Wong, M.; Bremner, T.; Sue, H.-J. Rheological and Thermal Behaviors of Commercial Poly(aryletherketone)s. *Polym. Eng. Sci.* **2013**, *53*, 651−661.
(49) Schmid, C. F.; Switzer, L. H.; Klingenberg, D. J. Simulations of Fiber Flocculation: Effects of Fiber Properties and Interfiber Friction. *J. Rheol.* **2000**, *44*, 781.
(50) Schmid, C. F.; Klingenberg, D. J. Mechanical Flocculation in Flowing Fiber Suspensions. *Phys. Rev. Lett.* **2000**, *84*, 290−293.
(51) Schmid, C. F.; Klingenberg, D. J. Properties of Fiber Flocs with Frictional and Attractive Interfiber Forces. *J. Colloid Interface Sci.* **2000**, *226*, 136−144.
(52) Switzer, L. H.; Klingenberg, D. J. Rheology of Sheared Flexible Fiber Suspensions Via Fiber-Level Simulations. *J. Rheol.* **2003**, *47*, 759.
(53) Switzer, L. H.; Klingenberg, D. J. Flocculation in Simulations of Sheared Fiber Suspensions. *Int. J. Multiphase Flow* **2004**, *30*, 67−87.
(54) Alig, I.; Skipa, T.; Engel, M.; Lellinger, D.; Pegel, S.; Pötschke, P. Electrical Conductivity Recovery in Carbon Nanotube−Polymer Composites after Transient Shear. *Phys. Status Solidi B* **2007**, *244*, 4223−4226.
(55) Kirkwood, J. G.; Auer, P. L. The Visco-Elastic Properties of Solutions of Rod-Like Macromolecules. *J. Chem. Phys.* **1951**, *19*, 281−283.
(56) Sun, D.; Chu, C. C.; Sue, H.-J. Simple Approach for Preparation of Epoxy Hybrid Nanocomposites Based on Carbon Nanotubes and a Model Clay. *Chem. Mater.* **2010**, *22*, 3773−3778.
(57) Liu, P.; White, K. L.; Sugiyama, H.; Xi, J.; Higuchi, T.; Hoshino, T.; Ishige, R.; Jinnai, H.; Takahara, A.; Sue, H.-J. Influence of Trace Amount of Well-Dispersed Carbon Nanotubes on Structural Development and Tensile Properties of Polypropylene. *Macromolecules* **2012**, *46*, 463−473.
(58) Stover, C. A.; Koch, D. L.; Cohen, C. Observations of Fibre Orientation in Simple Shear Flow of Semi-Dilute Suspensions. *J. Fluid Mech.* **1992**, *238*, 277−296.
(59) Petrich, M. P.; Koch, D. L.; Cohen, C. An Experimental Determination of the Stress−Microstructure Relationship in Semi-Concentrated Fiber Suspensions. *J. Non-Newtonian Fluid Mech.* **2000**, *95*, 101−133.
(60) Doi, M.; Edwards, S. Dynamics of Concentrated Polymer Systems. Part 1.—Brownian Motion in the Equilibrium State. *J. Rheol.* **1978**, *74*, 1789−1801.
(61) Doi, M.; Edwards, S. F. *The Theory of Polymer Dynamics*; Oxford University Press: New York, 1988.
(62) Barnes, H. Shear-Thickening ("Dilatancy") in Suspensions of Nonaggregating Solid Particles Dispersed in Newtonian Liquids. *J. Rheol.* **1989**, *33*, 329.
(63) Hoffman, R. L. Explanations for the Cause of Shear Thickening in Concentrated Colloidal Suspensions. *J. Rheol.* **1998**, *42*, 111−123.
(64) Forgacs, O.; Mason, S. Particle Motions in Sheared Suspensions: IX. Spin and Deformation of Threadlike Particles. *J. Colloid Sci.* **1959**, *14*, 457−472.
(65) Forgacs, O.; Mason, S. Particle Motions in Sheared Suspensions: X. Orbits of Flexible Threadlike Particles. *J. Colloid Sci.* **1959**, *14*, 473−491.
(66) Barber, A.; Kaplan-Ashiri, I.; Cohen, S.; Tenne, R.; Wagner, H. Stochastic Strength of Nanotubes: An Appraisal of Available Data. *Compos. Sci. Technol.* **2005**, *65*, 2380−2384.
(67) Sandler, J. K. W.; Kirk, J. E.; Kinloch, I. A.; Shaffer, M. S. P.; Windle, A. H. Ultra-Low Electrical Percolation Threshold in Carbon-Nanotube-Epoxy Composites. *Polymer* **2003**, *44*, 5893−5899.
(68) Gryshchuk, O.; Karger-Kocsis, J.; Thomann, R.; Konya, Z.; Kiricsi, I. Multiwall Carbon Nanotube Modified Vinylester and Vinylester-Based Hybrid Resins. *Composites, Part A* **2006**, *37*, 1252−1259.